Journal of Low Temperature Physics, Vol. 89, Nos. 5/6, 1992

The Superfluid Fraction of ^{3}He Confined in Pores of Sintered Silver

T. Hall,* S. M. Tholen,† K. R. Lane, V. Kotsubo, and J. M. Parpia**

Laboratory of Atomic and Solid State Physics, Cornell University, Ithaca, New York 14853-2501

(Received May 12, 1992; revised July 2, 1992)

We have measured the superfluid fraction of ^{3}He confined within the pores of silver sinter. Four sintered substrates were prepared with packing fractions between 23% and 68% of solid density. Measurements were carried out at six pressures between 0 bar and 29 bar. These results show that the superfluid fraction is suppressed to a much greater extent than expected.

1. INTRODUCTION

We describe measurements of the superfluid fraction of ^{3}He confined within the pores of sintered silver. Silver powders are commercially available in relatively small sizes. By packing them, it is possible to vary the mean pore size by a factor of five while maintaining some semblance of constancy in the basic structure of the sinter itself. The properties of ^{3}He within sintered silver are interesting for several reasons. These powders are commonly used as a thermal contact agent in cooling liquid ^{3}He samples to sub-millikelvin temperatures. The quality of the heat transfer process depends on the properties of the superfluid confined within it. Also, the ability to vary the packing fraction over a large range allows experiments to probe the effects of finite size since the characteristic grain and pore size are similar to the zero temperature coherence length.

The measurements span a wide range in pressure and pore sizes. The packing fractions were selected so as to provide nearly the maximum possible variation. The 23% packing fraction is close to the lowest possible mechanically stable configuration and the 68% sample approaches the limit of connectivity. We were able to observe superfluidity of ^{3}He confined within the pores of all of these samples.

*Present address: NASA/Goddard Space Flight Center, New York, N.Y. 10025.
†Present address: c/o Intel, Hillsboro, Oregon 97124.
**Present address: Conductus Inc., Sunnyvale, California 94086.

0022-2291/92/1200-0897$06.50/0

9. K. Ichikawa, S. Yamasaki, H. Akimoto, T. Kodama, T. Shigi, and H. Kojima, *Phys. Rev. Lett.* **58**, 1949, 1987.
10. A. F. Andreev, *Zh. Eksp. Teor. Fiz.* **46**, 1823, 1964, [*Sov. Phys. JETP* **19**, 1228, 1964].
11. N. A. Greaves and A. J. Leggett, *J. Phys. C* **16**, 4383, 1983.
12. J. M. Parpia, *Phys. Rev. B*, **32**, 7564, 1985.
13. D. I. Bradley, A. M. Guénault, V. Keith, C. J. Kennedy, I. E. Miller, S. G. Mussett, G. R. Pickett, and W. P. Pratt J., *J. Low Temp. Phys.* **57**, 359, 1984.
14. S. M. Tholen and J. M. Parpia, *Phys. Rev. Lett.* **67**, 334, 1991.
15. S. M. Tholen and J. M. Parpia, *Phys. Rev. Lett.* **68**, 2810, 1992.
16. E. V. Thuneberg, private communication.

the superfluid fraction increased by a factor of 1.7 in this cell after the addition of sufficient surface ^{4}He to alter the boundary condition.[16] We can only conclude that textural effects dominate in the most open geometry at high pressures and are comparable to effects from diffuse scattering in the most highly packed geometry. It is still true that there appears to be a considerable variation of the superfluid fraction with pressure at d/ξ_0 greater than ten, so the role of necks in controlling the flow cannot be discounted.

5. SUMMARY AND CONCLUSIONS

This data demonstrates that the properties of ^{3}He in sintered silver are quite complicated. In relatively open geometries, the superfluid fraction is suppressed by an amount considerably greater than expected. We attribute this to both the existence of necks with a range of diameters close to the coherence length as well as textural effects. The combination of small diameters and long coherence length serves to alter the path of the superflow and thus reduce the apparent superfluid fraction in a regime where the mean pore diameter is large compared to the coherence length. The existence of narrow pores which connect relatively open voids is important from the point of view of thermal transport in the sinter since the normal sections would function as sites for reflection of thermal excitations.

ACKNOWLEDGMENTS

This work contains input from a number of students over the years. Professor K. Hahn, Dr. J. DiTusa and Dr. R. Mihailovich all participated in different aspects of this experiment. The authors have benefitted from a number of interesting discussions with Dr. M. Freeman, Dr. E. Thuneberg, Dr. E. N. Smith, Professor V. Ambegaokar and Professor J. Reppy. Finally, the research was supported by the NSF through DMR 88-20170, DMR 91-23857 and the Cornell Materials Science Center through DMR 88-18588.

REFERENCES

1. Ulvac Vacuum Metallurgical Ltd., Shonan Building, 14010, 1 Chome, Chuoku, Tokyo, Japan.
2. Emerson & Cuming Inc., 869 Washington St., Canton MA 02021.
3. R. J. Roberston, F. Guillon, and J. P. Harrison, *Can. J. Phys.* **61**, 164, 1983.
4. P. A. Busch, S. P. Cheston, and D. S. Greywall, *Cryogenics* **24**, 447, 1984.
5. H. Franco, J. Bossy, and H. Godfrin, *Cryogenics* **24**, 477, 1984.
6. J. M. Parpia, W. P. Kirk, P. S. Kobeila, T. L. Rhodes, Z. Olejniczak, and G. N. Parker, *Rev. Sci. Instr.* **56**, 437, 1985.
7. D. S. Greywall, *Phys. Rev. B* **33**, 7520, 1986.
8. L. H. Kjaldman, J. Kurkijarvi, and D. Rainer, *J. Low Temp. Phys.* **33**, 577, 1978.

4.2. Relevance to Other Experiments

The existence of additional necks in the sample must have consequences on the thermal properties of the ^{3}He confined within the sinter. First, the effects of pair-breaking at the surface must result in regions which are rigorously normal in some of the necks between adjoining pores. The existence of such normal regions will create spatial variations in the order parameter. These spatial variations are likely to be smooth and occur over relatively short lengths. Nevertheless, the existence of such variations in the order parameter has been shown to cause anomalously low thermal conductivity in type II superconductors,[10] in which the vortex lattice plays the role of the necks in this geometry. Consequently, there is an exponentially damped transmission rate in the thermal transport of heat due to the spatial variation of the order parameter. This is due to the exponential decrease in the number of excitations with energy greater than the barrier height which is of the order of the energy gap, Δ. Calculations of this effect have been carried out by Greaves and Leggett,[11] and its consequences are noted in several papers in the literature.[12,13] However, this experiment provides new evidence for the existence and origin of these effects.

In a separate experiment,[14] we found that the addition of thin coverages of ^{4}He was able to alter the surface boundary condition for ^{3}He. Similar coverages were applied to the sintered silver in the 68% packing fraction cell.[15] We found that the surface boundry condition was altered. However, despite the ability to change the boundary condition, we found that the superfluid fraction was not restored to the full bulk value, but increased from $\sim$0.22 to $\sim$0.40 at 24 bar and $0.4T_c$. We attribute the incomplete restoration of the superfluid fraction to effects due to the variation of the $\boldsymbol{l}$ vector at the surface, whose gradient terms may still lead to a suppression of the superfluid fraction.[16]

The relative role of necks and textural contributions to the suppression of the superfluid fraction is difficult to assess since the effects are complementary. Theoretical estimates for the contribution of textural stiffness to the superfluid suppression are not available, but presumably these are only weakly pressure dependent. On the other hand, the geometry of these sinters is poorly known. The geometry of the 23% packing fraction cell is probably sufficiently open so as to ascribe all of the suppression at high pressure to textural effects. Thus the textural suppression is consistent with the expected $\sim\mu$m length scale associated with the characteristic bending radius of the $\boldsymbol{l}$ vector, providing we assume that the characteristic pore diameter is ≈ 1 μm. In the highly packed sinter, we note that the superfluid fraction does not appear to saturate as it did for the 23% packing fraction cell. Consequently, it is tempting to assign a large fraction of the suppression to the pair-breaking processes at the boundaries. This is consistent with our observation that

they were able to perform mercury intrusion porosimetry on the substrates, which yielded pore size distributions. The zero temperature coherence length (ξ_0) was calculated through a convolution of the measured superfluid fraction with the distribution of pore sizes and the expected suppression of the superfluid fraction by finite size effects. While the theoretical pressure dependence of ξ_0 was observed below 10 bar, the values at the higher pressures (>15 bar) do not decrease as much as expected, implying (as in our experiments) that the superfluid fraction continues to be suppressed in these relatively open geometries. Thus, in both these experiments, the superfluid fraction is suppressed to a greater extent than expected at short coherence lengths. We conclude that the simple intersecting pore model cannot adequately describe the variation of the pore sizes in the sinter.

4. DISCUSSION

4.1. Interpretation

The higher pressure, short coherence length data exhibits little variation of the superfluid fraction with pressure, and saturates at values considerably below unity for large d/ξ_0. At first examination, this behavior is seemingly at odds with measurements of the impedance to gas flow which were *smaller* than expected. Providing that the scattering is diffuse at the surfaces of the sinter, we would interpret the superfluid results as consistent with either a longer effective coherence length or smaller effective pore size.

An alternative explanation requires modification of the simple model for the sintered silver. The sinter may be better represented by a collection of voids connected by necks of much smaller diameter. If the diameter of the neck regions varies substantially, then the variation of the coherence length with pressure would strongly affect the χ factor. When the coherence length increases there are two effects. First, the superfluid fraction is suppressed within the voids. Second, because the coherence length may be larger than the neck diameter for a greater number of the necks, the effective path length that the superfluid has to follow increases, thus leading to a larger χ and a correspondingly smaller measured superfluid fraction.

Such a model has intuitive appeal. Clearly, there will be a distribution of neck sizes in the geometry, and χ_{eff} would exhibit a different pressure dependence for each of the packing fractions. We conclude that the original assumption (Sec. 2.2) of a single χ factor for each packing fraction is too simplistic to adequately model the behavior of superfluid ^{3}He in sintered silver.

of average pore diameter to coherence length. This temperature was selected since it is the lowest accessible at all pressures; also, the superfluid fraction should be close to its maximum value and $\xi(T) \approx \xi_0$. Thus virtually all of the temperature dependence should be eliminated. In this plot (Fig. 3) we show the variation of the superfluid fraction measured in each of the four cells. We expect that if the model accurately describes the pores in the sinter, then all of the data from the four different cells would collapse onto a single universal curve. Clearly, the data do not lie on a single curve. Rather, there are four different curves which exhibit some similarities. Most notable is the tendency of the superfluid fraction to saturate at shorter coherence lengths, manifested by the flattening of ρ_s/ρ observed at higher values of d/ξ_0.

A similar variation in the superfluid fraction is seen in the data of Ichikawa *et al.*[9] They measured the superfluid fraction in three packed alumina substrates with grain sizes of 3 μm, 1 μm, and 0.3 μm. The measured superfluid fraction varied from 8% in the small grain geometry at 0 bar to 65% in the large pore geometry at 20 bar, a range strikingly similar to that of our experiment. However, because of the material choice,

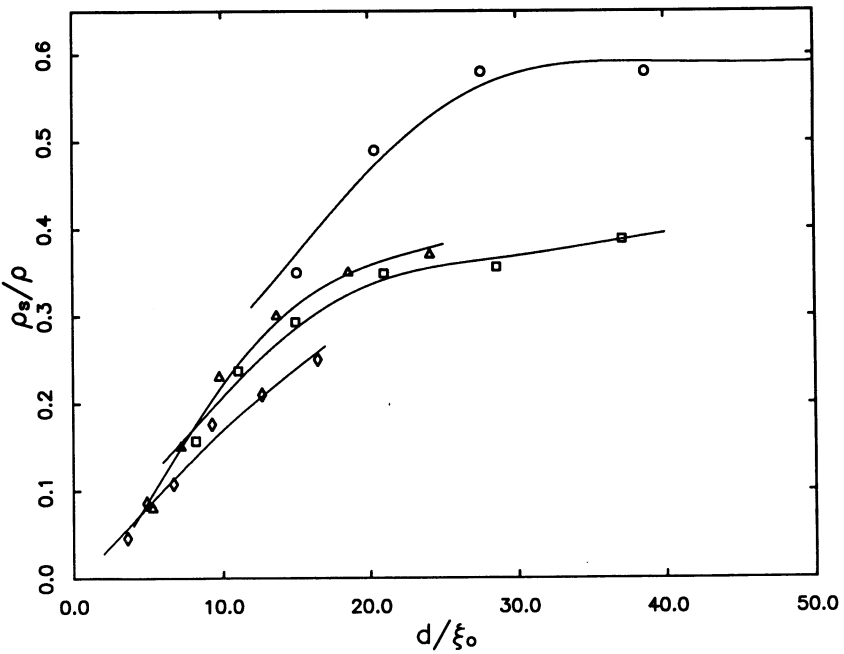

Fig. 3. The superfluid fraction at $0.35T_c$ for different pressures and packing fractions, plotted as a function of the pore diameter, d, normalized by the zero temperature coherence length, ξ_0, where the diameter was determined from the intersecting pore model. Symbols are the same as in Fig. 2. The solid lines are guides to the eye.

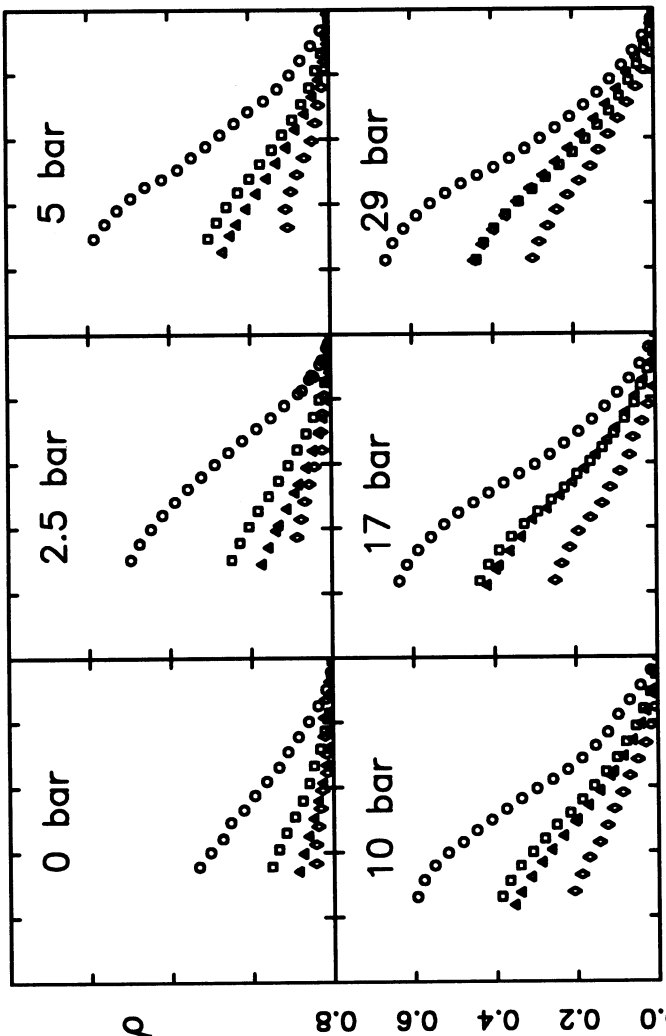

Fig. 2. Results for the superfluid fraction as a function of reduced temperature at six pressures between 0 and 29 bar. The symbols correspond to data from the 23% packing fraction cell (○), 40% (□), 54% (△), and 68% (◇) packing fraction cells. The scales for all the plots are identical to those of the labelled 10 bar data set.

expect from the theoretical results of Kjaldman *et al.*[8] that, providing the surfaces of the silver sinter are diffuse scatterers, the superfluidity of the ^{3}He would be suppressed within a coherence length of the surface. The zero temperature coherence length, ξ_0, is given by the relation $\xi_0 = \hbar v_F/2\pi k_B T_c$, and its values at various pressures are shown in Table 2. The pressures were selected to examine the superfluid density where the variation of the coherence length is the largest.

In Fig. 2, we plot the temperature dependence of the superfluid fraction measured in all of the four different cells at the six pressures. The results for the 68% cell show a suppression of the transition temperature. However, because of the distribution of pore sizes, the variation of the transition temperature from the bulk cannot be easily parameterized. The data points shown are representative of the full data set. The number of data points is about a hundred times larger than the number displayed.

Several features are noteworthy. The first is that there is a clear dependence of the superfluid fraction on the packing fraction. The second is that even at high pressures, where the coherence length is small compared to all of the pore diameters, the superfluid fraction never exceeds 0.65. We recall that the estimate pore size was 1.16 μm for the 23% cell. Thus, the ratio of pore diameter to coherence length (Table II) varies from 3.6 at low pressure for the 68% packing fraction cell to about 68 at high pressures for the 23% packing fraction cell. At such a large ratio of diameter to coherence length, we would expect the suppression of the superfluid fraction due to diffuse scattering events at the walls to be minimal. However, it is obvious that ρ_s continues to be suppressed substantially in this limit.

In order to emphasize this point, we have taken the measured values of the superfluid fraction at $T/T_c = 0.35$ and plotted them against the ratio

TABLE II
Measured and Derived Properties of Superfluid ^{3}He in Sintered Silver*

		P (BAR)	0	2.5	5	10	17	29
p(%)	d(μm)	ξ_0(Å)	770	570	420	300	220	170
23	1.16	$\rho_s/\rho(0.35\ T_c)$	0.33	0.48	0.56	0.56	0.57	0.61
		d/ξ_0	15	20	28	39	53	68
40	0.63		0.15	0.23	0.27	0.35	0.38	0.39
			8	11	15	21	29	37
54	0.41		0.08	0.15	0.23	0.30	0.35	0.37
			6	7	10	14	19	24
68	0.28		0.04	0.08	0.12	0.17	0.22	0.25
			4	5	7	9	13	17

* The table lists the superfluid fraction at $0.35T_c$ together with the zero temperature coherence length, ξ_0, and the ratio of pore diameter d (calculated from the intersecting pore model) to ξ_0 at the six pressures and for the four packing fractions.

diluted cerium magnesium nitrate) thermometer whose susceptibility was monitored using a SQUID. The LCMN salt was immersed in the liquid sample and was thermally well coupled to the torsional oscillators, while the coupling to the main heat exchanger was poorer. This was deliberate, so as to reduce thermal gradients between the LCMN and the oscillators. The helium was cooled by contact with a $\sim 25\ m^2$ heat exchanger formed by sintering copper flakes to the bulk copper body, which in turn was cooled through a compression joint by a praseodymium nickel demagnetization stage to below 0.5 mK.[6] Additional thermometry was provided through a melting curve cell mounted on the exterior of the copper body of the heat exchanger cell. The temperature scale was fixed by comparison to the melting curve and $T_c(P)$ as measured by Greywall.[7]

Data was taken by cooling the cryostat to approximately $0.3\ T_c$. Data collection proceeded by recording the temperature, period of the oscillator and the dissipation, though the latter did not provide any useful information except as an indicator of the transition temperature. The cell was heated so as to warm it at rates of approximately $0.02 T_c$/hr so that a typical warm-up would take between two to three days. This slow warm-up was required in order to maintain thermal equilibrium between different parts of the cell. We found that there were significant changes in the resonant period when the magnetic field on the nuclear stage was changed by more than $0.1 T$ and so we had to heat the nuclear demagnetization stage rather than remagnetize it in order to warm it. Small demagnetizations ($0.01 T$) were carried out to backtrack and recool the cell following a helium transfer. In this event, we were careful to have sufficient overlap in temperature so that any period shift could be properly normalized away. The magnitudes of such period shifts were small (typically less than a percent of the helium signal) since the magnitudes of the magnetic field changes were small.

We are confident that the LCMN thermometer accurately tracks the ^{3}He in the sintered silver cells since we observed no significant (<0.01 mK) temperature gradients between the experiments and the thermometer at the superfluid transition temperatures. We also found that if no heat was applied to the stage, the warm up rate was very low ($\sim 0.03 T_c$/day). Comparison of the superfluid fraction obtained at various rates of warming allowed us to increase the warming rate to $0.02 T_c$/hr. We also examined the superfluid fraction at various drive amplitudes in an unsuccessful effort to induce self heating. Consequently, we believe that the results presented in this paper are not the result of thermal gradients or offsets.

3.2. The Superfluid Fraction Results

We calculated the superfluid fraction from the period shift of the pendulum using Eq. (1) and the appropriate χ factor for each cell. We

attached to a beryllium copper torsion tube. This technique ensured minimal voids between the sinter and the epoxy and securely attached the sinter to the oscillator body. After the torsion rod was glued on, we drilled a 0.75 mm diameter hole through the length of the sinter from below (through the fill line in the torsion rod) in order to aid thermalization of the ^{3}He contained in the cell. The epoxy case had a pair of electrodes machined into its base which were coated with conductive point to form the moving plates of two capacitative drive and detection circuits. The experimental arrangement is shown in Fig. 1.

The experiments were carried out by mounting several torsional oscillators on a single platform so that data could be taken simultaneously. The experimental cells were located in close proximity to an LCMN (lanthanum

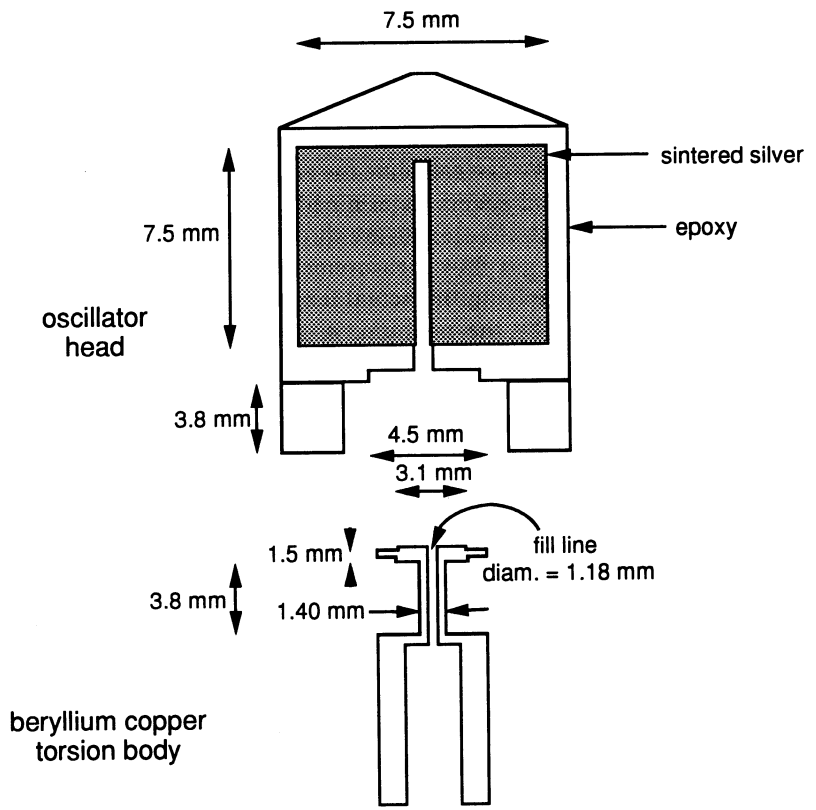

Fig. 1. A schematic depiction of the cell.

R/L demonstrates the shortcomings of this model since, taken literally, the intersection would constitute most of the open volume.

The measured surface area can be related to the packing fraction p through the relation

$$\sigma_A \equiv \text{Surface Area/Mass} = [3 \cdot 2R\pi \cdot (L-2R) + 4\pi R^2]/pL^3\rho$$

where the first term is the area of the three intersecting cylinders less the approximate area of intersection, and the second term is the area of the equivalent sphere at the intersection point. Here ρ is the density of silver. These relations serve to estimate the pore diameter. Clearly, the model depends a great deal on whether the intersections are complete or partial, and what the shape of the pores really is. So while exact equations for the intersecting pores' surface area could be developed, it is unlikely that they would be more relevant to the actual porous medium.

From the packing fractions and surface area measurements obtained from the BET analysis, we are able to determine the ratio of R/L and the values of L and R. These results are listed in Table I and show that the average pore diameter, d, varies with packing fraction from as large as 1.2 μm to 0.28 μm, approximately a factor in five variation.

The results can be compared to those obtained from flow measurements of gas through the pores. We can calculate the effective length of the sintered plug assuming the pore diameters determined from the intersecting pore model. The values of the effective length are shown in Table I. These effective lengths inferred from the gas flow measurements can be compared to the length computed by multiplying the actual length of the plug by the index of refraction introduced by the medium, n, given by $n = (1-\chi)^{-1/2}$. On comparing the two length scales, we find that the effective length is approximately a factor of three to five smaller than expected for all but the lowest packing fraction cell. This discrepancy is significant. We argue that such a short effective length is consistent with a more pictorial description of the sinter as a collection of spheres with the impedance being provided primarily by the necks between the larger interstitial voids. Thus, although the smallest pore diameter is much smaller than the average value, the effective length is considerably smaller and the impedance to gas flow is characteristic of a series of orifices. Such an interpretation is consistent with measurements of the superfluid fraction in the sinters.

3. EXPERIMENTAL DETAILS

3.1. Cell Construction and Experimental Details

Each of the four silver sinter substrates was first expoxied to seal the surfaces and then glued inside an epoxy sleeve which had been previously

$P(T)$, we measure the fraction of the fluid that is decoupled from the cell. Thus we form the ratio

$$\frac{\rho_s}{\rho} = \frac{1}{(1-\chi)} \frac{P(T_c)-P(T)}{P(T_c)-P(0)} \tag{1}$$

The χ factor is then found by setting this ratio equal to one. We measured values of χ (for ^{4}He) that ranged from 0.259 in the 23% sample to 0.636 in the 68% sample. These results are also shown in Table 1. Naively, for superfluid ^{3}He, one would expect the same χ since the geometry is identical. However, χ may be enhanced by pore size variations on the order of the coherence length since these would prevent superflow of ^{3}He through some pores, thus altering the geometry. The simplest model of the sinter (described below) accounts for the geometry by using the same χ found from ^{4}He experiments, and ascribes all the suppression of the superfluid fraction to finite size effects in the pore.

2.3. Model of the Sinter

Having completed the measurements on the sintered samples, we apply a simple model to estimate the pore diameter in each. Since the medium is quite inhomogeneous and not easily parameterized, these effective pore diameters are just estimates. Following earlier authors,[3] we began by setting up the intersecting pore model. Here the sinter is modelled by a series of three orthogonal cylindrical pores, arranged in a "jungle gym" configuration. The pores are assumed to be uniform and to intersect each other at a single node. Such a configuration leads to a unique determination of the pore diameter based on measurements of the surface area and packing fraction. We proceed with details of the calculation below.

Each of the three pores would have an open volume of $\pi R^2 L$, which would have to be modified due to the intersection between pores. The open volume is bounded by the limits $3\pi R^2 L - 8/3\pi R^3 < V < 3\pi R^2 L - 16R^3$. The lower bound is computed by subtracting the excess volume of the spheres of radius R and the upper bound is found from the excess volume from two cubes each of side $2R$. For simplicity, we set the open volume as $3\pi R^2 L - 4\pi R^3$, which is intermediate between these two values. Thus, in a cube of side L, there should be one set of such intersecting tubes. The open volume can be related to the packing fraction, p, through the relation

$$[3\pi R^2 L - 4\pi R^3]/L^3 = 1-p$$

$$\text{or} \quad 3\pi(R/L)^2[1-4/3(R/L)] = 1-p$$

For the various packing fractions we compute the values of R/L as lying between 0.46 for $p=0.23$ to $R/L=0.28$ for a packing fraction of 0.68. The values are listed in Table 1. The lowest packing fraction result of 0.46 for

of the samples were affected by the packing process. The results in Table 1 show that the areas decreased from 1.1 m^2/g for the 23% packing fraction to 0.65 m^2/g for the 68% packing fraction. This systematic decrease in surface area is qualitatively consistent with the micrographs. Comparable measurements have been carried out by other workers in the past[3,4,5] though not over as large a range of packing fractions.

We also measured the room temperature impedance of the sintered samples by packing them into pills which had effective dimensions of 0.635 cm diameter × 1.6 mm thick. Dry nitrogen gas was forced through the sinter at low pressures. Impedances ranged from 1.5×10^9 cm^{-3} for the 23% packing fraction sample to 3.6×10^{10} cm^{-3} for the 68% sample and are listed in Table I. These measurements were taken in an attempt to sample the effective diameter and length of the pores for flow. We reserve discussion on these results until later in this section.

Finally, the χ factor was measured by carrying out ^{4}He calibrations on the torsional oscillators described later in the paper. The χ factor is the parameter which quantifies the fractional mass of a superfluid that is entrained with the oscillator due to the tortuosity of the flow path. In relatively open geometries such as these sinters, there should be a negligible suppression of ^{4}He superfluidity due to finite size effects since the coherence length is on the order of a few Å. By measuring the empty cell period, $P(0)$, and the period of the oscillator above the superfluid transition temperature, $P(T_c)$, we obtain a calibration for the moment of inertia of the entire helium fluid mass. The viscous penetration depth exceeds the pore diameter and so we expect that the entire mass of the normal fluid is visciously coupled to the sinter. By cooling the cell to well below the superfluid transition temperature (below 1 K) and finding the period there,

TABLE I
Measured and Derived Parameters of Sintered Silver*

p	σ_A (m^2/g)	d (μm)	Z (cm^{-3})	L_{eff} (cm)	χ	n	L_{ex} (cm)
23%	1.1	1.16	1.5×10^9	0.133	0.26	1.16	0.18
40%	0.9	0.63	4.6×10^9	0.066	0.32	1.21	0.19
54%	0.8	0.41	8.4×10^9	0.034	0.53	1.46	0.23
68%	0.65	0.28	3.6×10^{10}	0.047	0.64	1.66	0.26

* Here p is the packing fraction, σ_A the surface area, d the inferred pore diameter using the intersecting pore model, Z the room temperature impedance of a 0.156 cm thick × 0.635 cm diameter sintered pill, L_{eff} the effective length of the sintered pill with a collection of pores of diameter d and impedance Z. The χ factor was determined from measurements of the ^{4}He superfluid fraction and n the index of refraction given by $n = (1-\chi)^{-1/2}$. L_{ex} is the length expected from the actual length multiplied by the index of refraction.

We have attempted to characterize the porous material. However, there are only a limited number of techniques to probe the properties of the material and each weights the properties differently. Consequently, only qualitative inferences can be made about the structure of the sinter. The paper starts by describing measurements that we have made to characterize the porous medium. We then describe the experimental set-up followed by the results, our interpretation and conclusions.

2. CHARACTERISTICS OF PACKED SILVER SINTER

2.1. Sample Preparation

All of the powder used in this study came from an old batch purchased from Ulvac[1] ten years ago, with a nominal size of 700 Å. The powder was packed by weighing out appropriate masses for the particular packing fraction in incremental packings of 1 mm height. The powder was packed in a stainless steel press which had a 0.75 cm diameter bore and a tight-fitting plunger. The press also served as the container in which the powder was sintered. The press was equipped with a detachable base to allow removal of the mechanically stable plug after sintering. The sample size was 0.75 cm diameter × 1 cm height, so the sinter was packed in ten increments. Each dose of sinter was added to the press and force applied on the plunger by a machinist's vise until the proper height was achieved. The force was not measured, but at the 68% packing fraction, was close to the limit that an individual could supply.

The plugs were placed in a vacuum oven, evacuated and heated to ~210°C over the course of ~100 minutes and maintained at this temperature for about an hour. Subsequent cool-down occurred over several hours. Plugs prepared for mounting into cells were then coated with epoxy (Stycast 1266[2]) that was partially cured to prevent it from being drawn into the pores by capillary action. Epoxy mixed between one-and-a-half to two hours prior to the application was found to have a suitable viscosity.

We also constructed several nearly identical sintered "pills" for characterization in an electron microscope. The micrographs reveal that the necks between adjacent particles become thicker as the packing fraction is increased. However, at the highest packing fraction fabricated (82%), it was clear that the structure was altered substantially with the pores being largely closed off. We did not attempt to measure the superfluid fraction in this highly packed sinter.

2.2. Sample Characterization

The sinters were characterized by carrying out BET isotherms at liquid nitrogen temperatures using nitrogen gas. We found that the surface areas